Photoacoustics 9 (2018) 1–9

Contents lists available at ScienceDirect

Photoacoustics

journal homepage: www.elsevier.com/locate/pacs

Research article

Laser scanning laser diode photoacoustic microscopy system

Mohsen Erfanzadeh[a], Patrick D. Kumavor[a], Quing Zhu[b,*]

[a] Department of Biomedical Engineering, University of Connecticut, Storrs, CT 06269, USA
[b] Department of Biomedical Engineering, Washington University in St. Louis, St. Louis, MO 63130, USA

ARTICLE INFO

Article history:
Received 7 July 2017
Received in revised form 21 September 2017
Accepted 16 October 2017
Available online 13 November 2017

Keywords:
Photoacoustic imaging
Diode lasers
Medical imaging
Biological imaging
Low-cost sources

ABSTRACT

The development of low-cost and fast photoacoustic microscopy systems enhances the clinical applicability of photoacoustic imaging systems. To this end, we present a laser scanning laser diode-based photoacoustic microscopy system. In this system, a 905 nm, 325 W maximum output peak power pulsed laser diode with 50 ns pulsewidth is utilized as the light source. A combination of aspheric and cylindrical lenses is used for collimation of the laser diode beam. Two galvanometer scanning mirrors steer the beam across a focusing aspheric lens. The lateral resolution of the system was measured to be ~21 μm using edge spread function estimation. No averaging was performed during data acquisition. The imaging speed is ~370 A-lines per second. Photoacoustic microscopy images of human hairs, *ex vivo* mouse ear, and *ex vivo* porcine ovary are presented to demonstrate the feasibility and potentials of the proposed system.

1. Introduction

Photoacoustic imaging (PAI) is a fast emerging imaging modality based on the thermoelastic induction of acoustic waves as a result of the absorption of pulsed or modulated optical energy [1–4]. Optical energy provides the excitation source and the induced acoustic waves are detected via ultrasound transduction [1]. Therefore, the difference in the absorption of tissue constituents provides the optical contrast in PAI.

Photoacoustic imaging is capable of mapping blood vasculature due to the higher absorption of hemoglobin compared to other tissue constituents in the visible and near infrared (NIR) wavelength ranges [1,5]. Angiogenesis, which is the irregular growing of vasculature in the tumor area, is a significant indicator of cancer development [6–10]. Hence, photoacoustic tomography (PAT) and photoacoustic microscopy (PAM) have been utilized in oncology [11,12] for cancer detection and treatment monitoring via mapping tumor angiogenesis in breast [13,14], prostate [15–17], skin [18–20], thyroid [21,22], colorectal [23–25], pancreatic [25], cervical [26], and ovarian cancer [27–32].

Out of the 30 different types of ovarian cancer, almost 90% of the cases are epithelial ovarian cancer, which originates from the cells covering the outer surface of the ovary. Unfortunately only about 30 percent of epithelial ovarian cancer cases are diagnosed at early stages [10,33,34]. Currently, the standard of care is removal of ovaries of high risk patients. This procedure, however, increases the mortality rate of young women [35], and therefore, the development of methods to reduce unnecessary surgeries is critical. Given the significance of angiogenesis in epithelial ovarian cancer [8], Wang et al. demonstrated the potential of a PAM image feature extraction algorithm for classification of normal and malignant *ex vivo* ovarian tissues [27].

However, that PAM system included a solid-state laser system (*i.e.* Ti-Sapphire laser pumped by a second harmonic Nd:YAG laser (LT2211 and LS-2134, Symphotics TII Corp, Camarillo, CA)) and a high precision 3-D linear motor [27]. The system was not only expensive and bulky but also slow on data acquisition. Solid-state lasers can be more compact and fast; however, the cost is still high with prices in the range of $15 K–$40 K. Low-cost and compact PAM systems will facilitate the transition from laboratory tools to clinical devices. There are many clinical applications that could potentially benefit from low cost, compact and fast photoacoustic microscopy and endoscopy systems such as ovarian cancer [27], skin cancer [18–20], cervical cancer [26,36,37], and colon cancer [23–25] detection and diagnosis. The importance of developing low-cost, compact, and fast photoacoustic imaging systems for enhancing the clinical applicability of photoacoustic imaging in oncology has been emphasized by other researchers as well [11]. Low-cost photoacoustic imaging systems can also encourage biomedical photoacoustic research in developing countries. Additionally, considering the applications of PAI in oncology and the importance of access to affordable medical devices in low-

* Corresponding author.
E-mail address: zhu.q@wustl.edu (Q. Zhu).

https://doi.org/10.1016/j.pacs.2017.10.001

income countries as stated by the World Health Organization (WHO) compendium of innovative health technologies for low-resource settings, low-cost PAI systems can potentially benefit the realization of Universal Health Coverage (UHC) [38].

High-power pulsed laser diodes (PLD) have been used as low-cost and compact substitutes for light sources both in PAM and PAT [39–46]. Wang et al. presented a low-cost laser diode-based PAM system with a 905 nm PLD as the excitation source. However, the signal-to-noise ratio (SNR) and imaging quality of the system was limited mainly due to the optical energy loss in a 60× microscope objective [41,42]. Moreover, the need for 128 signal averaging limited the imaging speed of the system. Zeng et al. demonstrated a laser diode based PAM system with a 405 nm PLD as the excitation source which required 512 averaging and had a low imaging speed [43]. Li et al. presented a laser diode based PAM system with a Blu-ray DVD pickup head as the excitation source [45]. This system also required 3000 times averaging for imaging biological tissues. We previously reported a method to obtain a low-loss collimation and focusing for a 905 nm high power PLD that enabled obtaining PAM images of porcine ovarian tissue [42]. However, the aforementioned system also suffered from a low imaging speed. Moreover, the laser diode based PAM systems mentioned above require mechanical scanning of the sample which limits potential clinical applications.

Moving toward clinical *in vivo* PAM applications requires rapid image acquisition. However, rapid image acquisition also benefits *ex vivo* clinical and research applications. This is because incised samples should be fixed in formalin soon after the incision in order to preserve the freshness for histology, thus providing only a short imaging time window after the surgery. Faster *ex vivo* imaging will hence better preserve the sample freshness and morphological information prior to formalin fixation [47]. Here, for the first time to the best of our knowledge, we present a fast laser scanning laser diode-based photoacoustic microscopy system. No averaging is used for obtaining the images. The imaging speed is 370 A-lines per second. The long-reach and low-loss collimation of the PLD beam needed for laser scanning is achieved using a combination of aspheric and cylindrical lenses. Two galvanometer scanning mirrors perform the two-dimensional scanning of the beam across an aspheric focusing lens, hence no need for mechanical scanning of the sample. Photoacoustic microscopy images of human hairs, *ex vivo* mouse ear, and *ex vivo* porcine ovary are presented to demonstrate the feasibility of the proposed system for imaging and characterizing biological tissues. The capability of imaging the thin

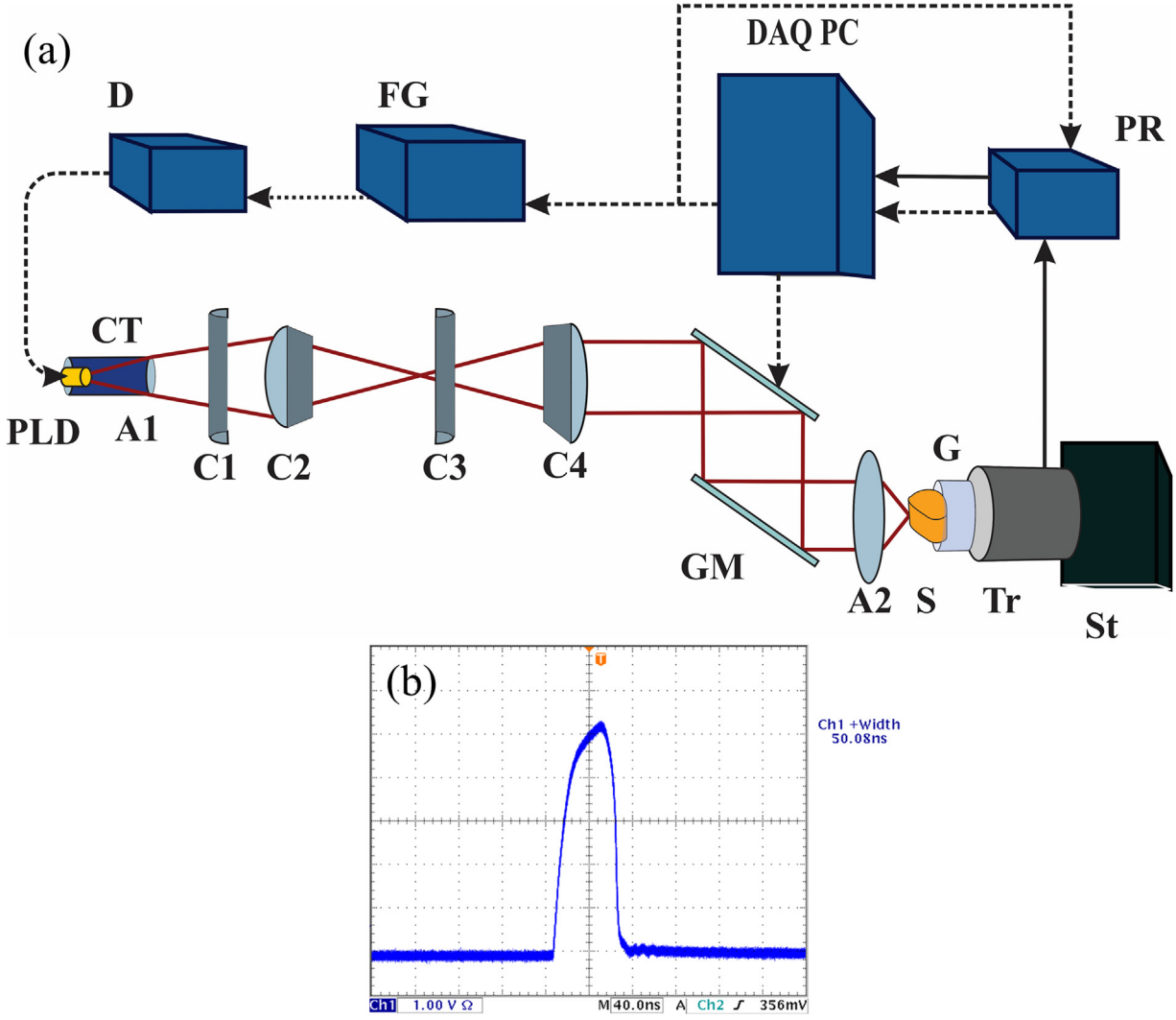

Fig 1. (a) Schematic of the laser scanning laser diode based photoacoustic microscopy system. The dashed arrows represent trigger and control signals and the solid arrows represent PA signal transfer. (b) Pulsewidth of the PLD light is ~50 ns.

vasculature on porcine ovarian tissue suggests the potential of the proposed low-cost and fast PAM system for characterization and classification of ovarian tissue [27].

2. Materials and methods

2.1. Laser scanning laser diode photoacoustic microscopy setup

The schematic of the laser diode based photoacoustic microscopy system is depicted in Fig. 1(a). A 905 nm (±10 nm), 325 W maximum output peak power pulsed laser diode (Laser components, 905D5S3J08S) is utilized as the excitation source. The laser is pulsed by a PLD driver (D, PicoLas LDP-V 240-100 V3) with 50 ns pulsewidth (Fig. 1(b)).

In order to perform laser scanning, the PLD light has to be well collimated for a reasonably large distance. However, the multiple active elements in high power stacked PLDs and the intrinsic anisotropy of their beam [42,48] are challenges for maintaining a low-loss collimation of the light. The PLD used in this system has a 200 × 440 μm emitting area. It consists of five active areas, each 200 μm wide. The active areas are stacked vertically with 110 μm vertical separation between consecutive ones. The PLD is first placed inside a collimation tube (CT) with an aspheric lens (A1, Thorlabs, A230TM-B) in order to improve the collimation. This, however, is not sufficient because of the short focal length of the lens, and the rather large vertical separation between the active elements and beam divergence angle. Therefore, to further improve the collimation, four cylindrical lenses are utilized. Two of these lenses (C1 and C3, Thorlabs, LJ11878L2-B and LJ1821L1-B, respectively) act as a Keplerian beam expander in the slow axis direction, and the other two (C2 and C4, Thorlabs, LJ1212L1-B and LJ1105L1-B, respectively) act as a Keplerian beam expander in the fast axis direction. Fig. 1(a) only shows the changes in the beam in the fast axis direction as the slow axis direction has no vector components in the plane of this two-dimensional illustration. After passing through C4 the entire beam maintains its initial 17 × 12 mm size for more than 30 cm until it reaches the scanning mirrors and the focusing lens. Two galvanometer scanning mirrors (GM, GSI Group, G330) are used to scan the beam across a 1- inch diameter aspheric lens (A2) with a numerical aperture (NA) of 0.71 (Edmund optics, 66-020) which focuses the beam on the sample (S). The generated photoacoustic (PA) signal is detected by an unfocused ultrasound transducer (Tr) with a center frequency of 3.5 MHz and a bandwidth of 60% (Echo, BI933). Ultrasound gel (G) is used for coupling the PA signal between the sample and the transducer. The transducer and sample are placed on a three-dimensional stage (St) for positioning of the sample.

2.2. Data acquisition and processing

The PA signal is amplified by an ultrasound pulser and receiver (PR, Panametrics, 5072PR) with 59 dB gain and is digitized by a 65 MHz, 14-bit data acquisition (DAQ) card (Gage-applied, GS8325). The mirrors and the data acquisition card are synchronized by the DAQ PC. A 16-bit multifunction data acquisition card (National Instruments, PCIe 6251) provides a finite number of 1 KHz trigger pulses to a function generator (FG) that feeds the PLD driver. The same trigger signal is sent to the ultrasound receiver. The B-scan signal of the x-axis mirror is a ramp signal from the multifunction DAQ card and it starts and finishes in synchrony with the beginning and end of the trigger pulse train. A-lines are acquired via a multiple acquisition scheme. A-line data are triggered by the trigger output of the ultrasound receiver, stored in the circular buffer of the Gage DAQ card, and transferred to the PC after a B-scan is finished. The y-axis mirror moves in a step-wise fashion after the B-scan data acquisition and saving is performed. Control, data acquisition, and signal processing to form maximum intensity projection (MIP) images are performed in a single code in MATLAB (MathWorks, Natick, Massachusetts, USA). No averaging is performed on the A-line signals. A MATLAB built-in moving average filter is performed on the raw A-line signals to slightly remove the high frequency noise (higher than 8 MHz) and improve the SNR. The final image undergoes a MATLAB built-in median filter. The final imaging speed is approximately 370 A-lines are per second. Therefore, for instance, a 500 × 200-pixel image can be acquired and displayed in approximately four and a half minutes.

3. Results

3.1. Lateral resolution

The maximum field of view was measured by imaging targets of known sizes and comparing the size of their image to the field of view. A maximum field of view of approximately 4.6 mm × 3.7 mm ±0.3 mm was obtained. Several measurements were performed and the average value is reported.

The lateral resolution was measured to be approximately 21 μm using edge spread function estimation. The edge of a high contrast target (black tape) was imaged and the one-dimensional cross-sectional profile of the image was fitted by an error function, which is considered as the edge spread function (ESF). The first derivative of the ESF represents the line spread function (LSF) and the full-width-at-half-maximum (FWHM) of the LSF represents the lateral resolution [49,50]. Fig. 2(a) shows the PAM image of the edge of the high contrast target. Fig. 2(b) depicts the measured edge response along the dashed line in Fig. 2(a), the fitted ESF, and the corresponding LSF. The pixel size in Fig. 2(a) is 0.125 × 6.7 μm in horizontal and vertical directions, respectively. The pixel sizes are governed by the scanning area and the number of A-lines per B-line for the horizontal direction and the number of B-lines for the vertical direction.

3.2. Axial resolution

The theoretical axial resolution as derived from the ultrasound transducer is given as 0.88 c/B, where c is the speed of sound in tissue (~1540 m/s) and B is the bandwidth of the transducer [51]. With a 3.5 MHz central frequency and 60% bandwidth (corresponding to 4.1 MHz), the theoretical acoustic axial resolution is ~331 μm. Fig. 3(a) shows the PAM image of a thin human hair. The pixel size in Fig. 3(a) is 0.836 × 2.1 μm in horizontal and vertical directions, respectively. As shown in Fig. 3(b), FWMH of the one-dimensional cross-section of the image along the dashed line is approximately 35 μm. Fig. 3(c) shows the A-line signal from the thin hair target and its envelope obtained from Hilbert transformation. FWHM of the envelope is ~220 ns, corresponding to an ~339 μm axial resolution [51], which is very close to the theoretical value. Due to the limited axial resolution of the transducer compared to the lateral resolution, only 2D images are presented in this report. It should be noted that with higher pulsewidths, axial resolutions larger than the theoretical value were obtained, and this would further limit the ability to separate targets at different depths.

3.3. Depth of penetration

In order to assess the penetration depth, a black human hair is inserted approximately two millimeters below the surface of a chicken breast and another black human hair is inserted just below the surface to serve as the reference point for depth measurement. Fig. 4(a) and (b) show the side and overhead views of the chicken breast piece, respectively. Fig. 4(c) shows the maximum intensity

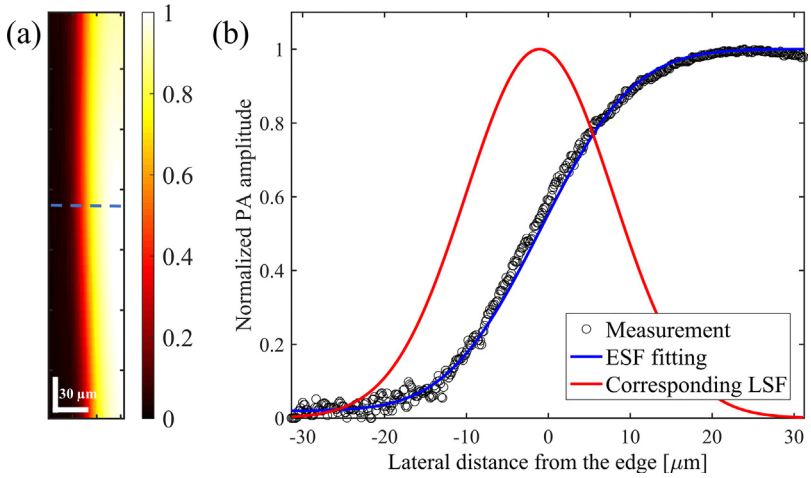

Fig. 2. (a) PAM image of the edge of a high contrast target. The color bar represents normalized PA amplitude. (b) The one-dimensional cross-sectional profile of the image along the dashed line, the ESF, and the LSF. FWHM of the LSF is approximately 21 μm.

projection image of the two hairs and Fig. 4(d) shows the B-line image along the dashed line in Fig. 4(c). The 2-mm axial distance between the hairs is apparent in Fig. 4(d) and the SNR, 20 log (Vsignal/Vnoise), of both hairs is slightly higher than 6 dB. It should also be noted that the hair close to the surface (on the left side of the image in Fig. 4(c)) appears thicker than the deeper hair (on the right side of the image in Fig. 4(c)) because the focal spot is set to be closer to the 2-mm deep hair and the hair close to the surface is out of focus considering the 0.71 NA of the focusing lens. The pixel size in Fig. 4(c) is 3.1 × 4.2 μm in horizontal and vertical directions, respectively. The pixel size in Fig. 4(d) is 3.1 × 23.6 μm in the horizontal and axial directions, respectively. The axial pixel size is governed by the 65 MHz sampling of the data acquisition card and assuming 1540 m/s speed of sound in the tissue.

3.4. PAM image of human hairs

PAM image of black human hairs positioned to form multiple branches is depicted in Fig. 5(a) in order to demonstrate the imaging of branch-shaped targets. The hairs were measured to be thinner than 100 μm using a standard caliper. The one-dimensional cross-sectional profile of the image along the dashed line is presented in Fig. 5(b). FWHM of profiles range between 80 μm to 180 μm. Hairs with thicker profiles in the image were positioned slightly out of focus. The pixel size in Fig. 5(a) is 6.7 × 18.5 μm in horizontal and vertical directions, respectively.

To further demonstrate the capability of imaging branch-shaped targets lying deep in the tissue, crossing black human hairs inserted about 1 mm below the surface of a chicken breast were imaged. Fig. 6(a) and (b) show the side and overhead views of the chicken breast piece and Fig. 6(c) shows the PAM image of the hairs. The hairs are clearly resolved with ~15 dB SNR. The pixel size in Fig. 6(c) is 8.3 × 8.4 μm in the horizontal and vertical directions, respectively.

3.5. PAM image of mouse ear ex vivo

Ex vivo PAM image of a mouse ear and its photograph are presented in Fig. 7(a) and (b), respectively. Mouse ears were obtained from the University of Connecticut animal facility and the institutional oversight was waived. The thin vessels inside the rectangle are all resolved in the image, even the vessels that have lost blood during the incision and appear less clear in the photograph. The pixel size in Fig. 7(a) is 5 × 12.3 μm in horizontal and vertical directions, respectively. PAM image of another *ex vivo* mouse ear and its photograph are presented in Fig. 7(c) and (d), respectively. As it can be seen from the photograph, the ear was imaged from inside rather than outside so that the vessels on the left side of the rectangle in Fig. 7(d) lay deeper in the tissue. However, these vessels, as indicated by solid arrows, are clearly resolved in the image. Moreover, the areas where blood is not continuous in the vessel, as indicated by dashed arrows, are

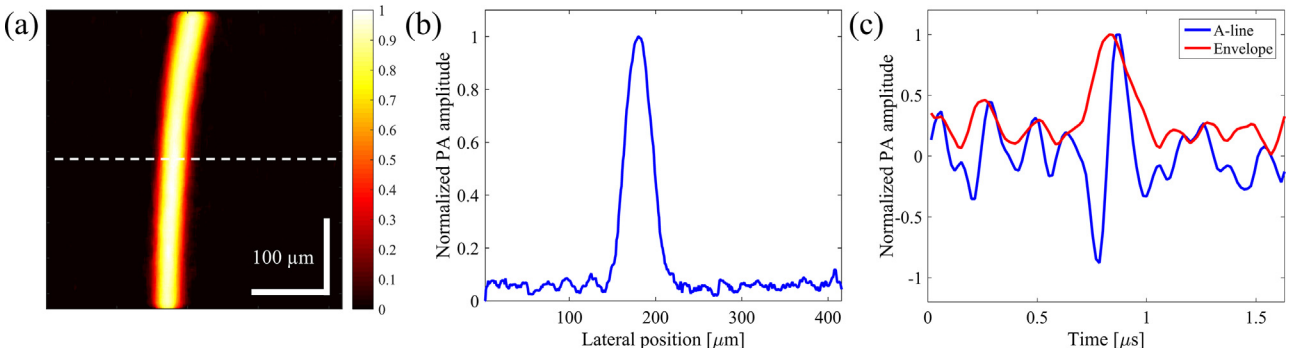

Fig. 3. (a) PAM image of a thin human hair. The color bar represents normalized PA amplitude. (b) One dimensional cross-sectional profile of the image in (a) along the dashed line shows ~35 μm thickness. (c) A-line signal from the hair and the corresponding envelope. FWHM of the envelope is ~220 ns, corresponding to ~339 μm axial resolution.

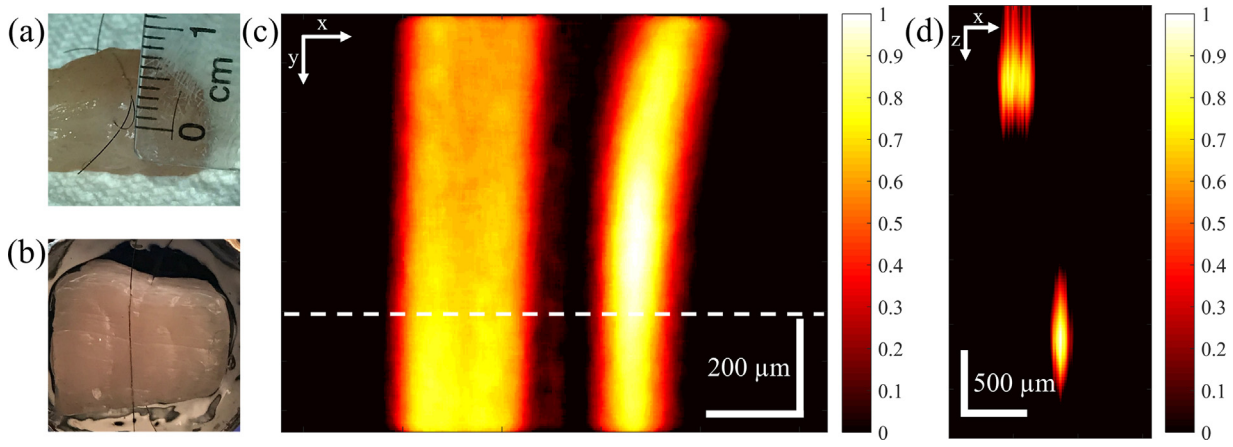

Fig. 4. (a) Side view of chicken breast piece used for depth of penetration measurement (b) Overhead view of the chicken breast piece (c) Maximum intensity projection PAM image of the hairs inside the chicken breast. The hair on the left side of the image is close to the surface and the hair on the right side of the image is about 2 mm deep. (d) B-line image along the dashed line in Fig. 4(c). Color bars represent normalized PA amplitude.

distinguished with details. The pixel size in Fig. 7(c) is 4.4 × 6.9 μm in horizontal and vertical directions, respectively. The SNR for imaging mouse ear *ex vivo* is ∼14 dB.

3.6. *PAM image of porcine ovary* ex vivo

To evaluate the capability of the system for imaging ovarian tissue, a porcine ovary was imaged *ex vivo*. Porcine ovaries were obtained from a local farm and the institutional oversight was waived. PAM image of the *ex vivo* porcine ovary and its photograph are presented in Fig. 8(a) and (b), respectively. As can be seen, the system is capable of resolving thin vessel branches that are positioned under the tissue surface and are not apparent in the photograph. The pixel size in Fig. 8(a) is 2.9 × 10.1 μm in horizontal and vertical directions, respectively. The SNR for imaging porcine ovary *ex vivo* is ∼18 dB.

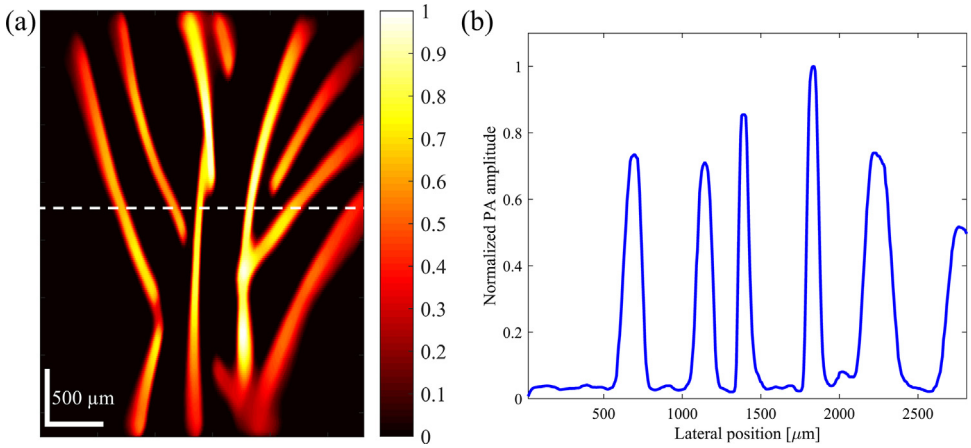

Fig. 5. (a) PAM image of human hairs. The color bar represents normalized PA amplitude. (b) One-dimensional cross-sectional profile of the image in (a) along the dashed line.

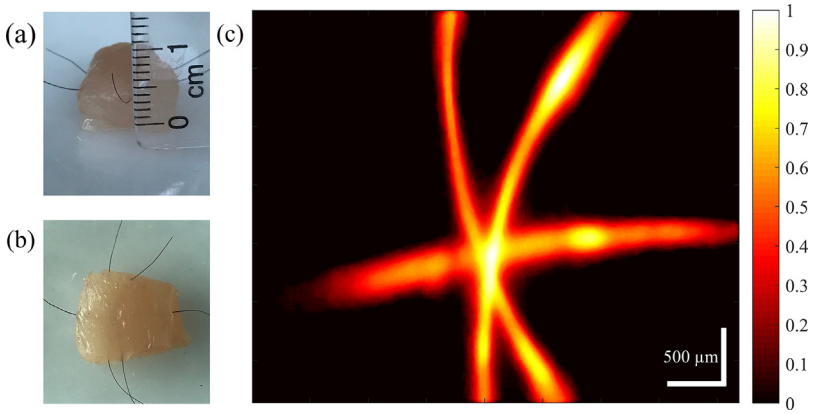

Fig. 6. (a) Side view of chicken breast piece with crossing hairs inserted ∼1 mm below the surface (b) Overhead view of the chicken breast piece (c) PAM image of the crossing hairs inserted ∼1 mm below the chicken breast surface.

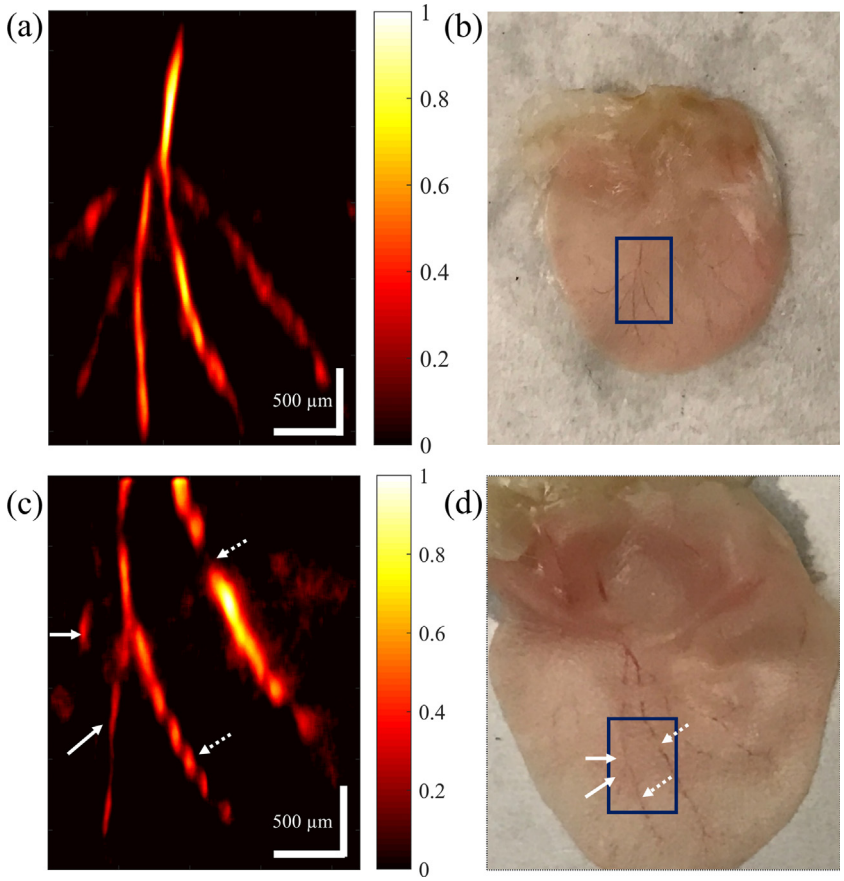

Fig. 7. (a) and (c) PAM image of the vasculature on a mouse ear *ex vivo*. The color bars represent normalized PA amplitude. (b) and (d) Photograph of the mouse ear in (a) and (c), respectively.

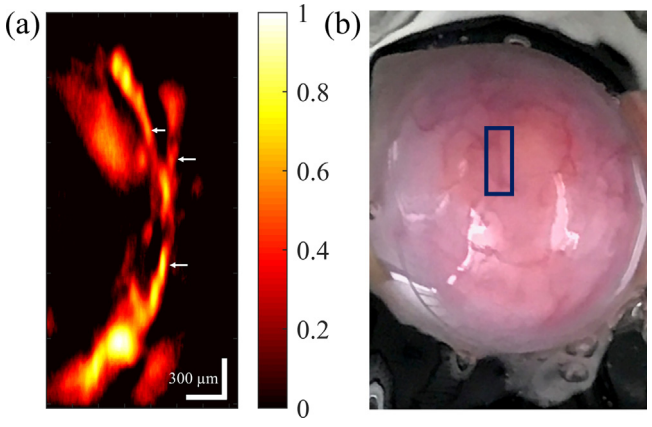

Fig. 8. (a) PAM image of the vasculature on a porcine ovary. The color bar represents normalized PA amplitude. (b) Photograph of the porcine ovary.

FWHM of the vessel branches indicated by the arrows in Fig. 8(a) are 50–65 μm. Considering the ability to resolve such vessels on the porcine ovary and the ~21 μm resolution, the system shows potential sensitivity to arterioles, venules, angiogenic sprouting clusters, and micro-vessel clusters, which are present in tumor angiogenesis [6,8,31,52–56]. Also most of the vasculature in the sample PAM images of normal and malignant ovarian tissue presented in Ref. [27], where the authors use feature extraction of PAM images to classify normal and malignant ovarian tissues, are of similar or larger sizes [27]. The FOV of the presented ovarian tissue PAM image is ~1.5 mm × 3 mm. Such an area can potentially contain part of the vasculature feeding or surrounding a tumor site. Therefore, when combined with feature extraction algorithms to analyze the configuration and distribution of the vasculature [27], the proposed low-cost and fast laser diode based laser scanning photoacoustic microscopy system has the potential of imaging and classification of ovarian cancer, providing an important step towards the clinical application of PAM for studying ovarian cancer.

4. Discussion

The proposed PAM system offers significant improvement in the imaging speed compared to previously reported low-cost laser diode-based PAM systems [39–43], eliminates the need for mechanical scanning of the sample, and has demonstrated the potential for imaging and classification of ovarian tissue. Even though laser scanning PAM systems utilizing conventional solid-state lasers with comparable or higher speeds have been reported previously [57,58], this is the first implementation of a fast laser scanning PAM system using a low-cost and small pulsed laser diode. The PLD used in this paper is approximately $540 and the PLD driver is approximately $1350, resulting in a total of $1890, which is significantly lower than the cost of conventional photoacoustic light sources. The proposed system is therefore one step closer to low-cost, compact, and fast PAM devices valuable for clinical use.

A PAT system using a pulsed laser diode as the excitation source (lateral resolution of 180 or 380 μm with a 5 MHz or 2.5 MHz transducer, respectively) has been developed by other researchers

[44]. The cost of the PLD used in the PLD-PAT system is ~$15 k [44]. Therefore, given that the system proposed here is much less expansive and yet can provide ~21 μm lateral resolution makes it worthwhile to use. Additionally, to obtain a lateral resolution of 21 μm with acoustic resolution PAM, the required frequency of the focused ultrasound transducer should be higher than 75 MHz [59]. Such transducers (especially focused ones) are not commercially available and are very expensive if custom designed. For instance, several examples of acoustic resolution PAM using conventional light sources have used a transducer with 50 MHz central frequency and 70% bandwidth with a lab-made acoustic lens of 0.44 numerical aperture and have reported 45 μm lateral resolution [19,20,60,61]. Currently, we are not aware of any acoustic resolution PAM systems utilizing low-cost PLDs.

The theoretical diffraction limited resolution of optical resolution PAM is estimated as 0.5 λ/NA, where λ is the wavelength and NA is the numerical aperture of the lens. With a 905-nm wavelength and 0.71 numerical aperture, the diffraction limited resolution is 0.63 μm, which is much smaller than the resolution obtained in this setup. In order to reach the diffraction limit, the laser light should have a Gaussian profile and it should have a very small divergence angle. Using fast/slow axis microlens collimators can improve the beam profile, collimation, and consequently the focusing [62]. Also, using beam expanders with larger expansion ratios can further decrease the divergence angle and improve the collimation and focusing. However, this will increase the beam size and results in more light energy loss due to the limited aperture of the scanning mirrors and the focusing lens. As a future work, a single, small, two-dimensional microelectromechanical system (MEMS) based actuator can be used for laser scanning. Such a scanning mirror can be placed after the focusing lens, therefore light will be scanned after the focusing lens rather than inside it. As a result, the beam can be further expanded before reaching the lens, leading to a smaller divergence angle and a better focusing. It should also be noted that although the focusing lens in this report is a single aspheric lens and introduces less aberrations compared to spherical lenses, it is estimated that the resolution degrades about 20–30 μm near the edges. Using a specific scanning lens (f-theta, *etc.*) can provide a flatter focal plane for all scanning angles and maintain a fairly similar focal spot even near the edges. However, the relative high cost of such lenses, especially with numerical apertures as high as 0.71, may affect the low-cost nature of the system.

Using visible pulsed laser diodes (*e.g.* 405 nm) would potentially improve the lateral resolution. However, NIR light demonstrates better penetration depth in optical resolution PAM compared to the visible range [63], which enhances the potential to image vessels lying deeper beneath the surface of the ovarian tissue. Moreover, although the absorption coefficient of hemoglobin is higher in 405 nm compared to 905 nm, available energies of NIR PLDs are higher than those in the visible range [5,43,45]. Light emitting diodes (LEDs) have also been reported as photoacoustic light sources [64,65], however due to the larger divergence of LED beam compared to laser diodes, it is more challenging to obtain low-loss collimation and tight focusing of LED beam [65]. Moreover, PLDs can have shorter pulsewidths compared to LEDs, which leads to better axial resolution [65].

In order to obtain better axial resolution for high resolution 3D imaging, higher frequency ultrasound transducers can be employed. Because in this system PA signals are detected in transmission mode and healthy human ovaries are 1.5–2 cm thick and diseased ones can have larger sizes [66], we have used a relatively low-frequency ultrasound transducer to avoid attenuation of ultrasound waves travelling in the tissue. Considering the current SNR level for ovarian tissue imaging, attenuation caused by higher frequency transducers in the transmission mode will affect the image quality. Higher frequency transducers can be used in a reflection mode PAM setup that does not require the ultrasound waves to pass through the tissue. It has also been shown that application of Wiener deconvolution on the axial direction can provide ~1.7 times improvement in the axial resolution [51]. Moreover, an unfocused transducer is used in the current system because while light is scanned on the sample, the ultrasound transducer is stationary. If a focused transducer is used, the detection sensitivity decays rapidly away from the focal spot, hence limiting the field of view. Using a focused transducer confocal with the optical excitation, which is common in reflection mode PAM systems, can potentially provide about 20 dB increase in the detected PA signal level [57,67,68]. It should be noted that considering the limited photoacoustic signal level, in order to maintain sufficient SNR without averaging in the reflection mode PAM, efficient coupling of the ultrasound signal to the transducer is necessary. Due to the properties of the PLD, a high numerical aperture lens (1-inch diameter, 17.5 mm focal length, 0.71 NA) is required to reach the desired resolution in the current setup. In the reflection mode laser scanning PAM systems, either the transducer is placed confocal with the optical focus and both light and acoustic wave are steered by the mirror [57], or the transducer is tilted with respect to the sample [58]. In both forms, low numerical aperture lenses (NA ~0.1, focal length 50 mm [57] or 60 mm [58]) are used so that either there is enough space for the mirror and beam combining components between the lens and the sample [57] or the transducer has a small degree with respect to the sample (30 mm away, 15° tilted [58]). Therefore, achieving acceptable resolution and efficient ultrasound signal coupling is a challenge that should be addressed in future reflection mode laser scanning laser diode PAM systems. Improving the beam profile and collimation will allow achieving acceptable lateral resolution with lower numerical aperture lenses, hence paving the way for the reflection mode configuration.

The light energy directly from the PLD (without the optical system) was measured to be approximately 16 μJ and the energy delivered to the tissue was measured to be approximately 13 μJ. Assuming the focal spot to be 0.5–2 mm below the surface of the sample, the maximum surface optical fluence is estimated to be between 1.6–0.1 mJ/cm^2, which is far below the maximum permissible exposure (MPE) at this wavelength according to the American National Standards Institute (ANSI) safety standard [69].

Imaging and classification of normal and malignant human ovaries using the proposed system is a future task. The imaging speed can also be further increased. The maximum repetition rate of this PLD is governed by its absolute maximum duty cycle of 0.1%. Therefore, at 50 ns or lower pulsewidths the repetition rate can be increased up to 20 KHz. Considering that no averaging is required in this system, using an improved data acquisition scheme and up to 20 KHz repetition rate of the PLD, the imaging speed can be significantly increased. A laser scanning laser diode-based PAM system using a MEMS-based two-dimensional actuator with improved imaging speed is currently under development to obtain better image quality and imaging speed and move towards a reflection-mode setup.

Furthermore, development and application of photoacoustic contrast agents with absorption peaks near 905 nm can enhance the SNR and image quality of this system [70–74]. Studying skin and cervical cancer can be other possible applications of a laser scanning laser diode based PAM system [18–20,26]. With further developments, endoscopic laser diode-based photoacoustic microscopy systems have great potential to provide angiogenesis distribution of ovarian surface during minimally invasive surgery which can guide surgeons to reduce unnecessary surgeries [27]. Such systems also have great potentials for diagnosis of colorectal [23–25], pancreatic [25], and esophageal [75] cancer.

5. Summary

A low-cost and fast laser scanning laser diode based photoacoustic microscopy system is presented. The lateral resolution is approximately 21 μm. PAM images of human hairs, *ex vivo* mouse ear, and *ex vivo* porcine ovary have been presented. The imaging speed is significantly higher than previously reported laser diode-based PAM systems and the need for mechanical scanning is eliminated. The results indicate the potential of the proposed method for *in vivo* imaging of biological tissues.

Conflict of interest

The authors declare that there are no conflicts of interest.

Acknowledgements

This research was supported by NIH R01CA151570. The authors would like to thank Feifei Zhou and Kimberlie Davenport from University of Connecticut for helping with biological sample preparation. We would also like to thank E&J farms at Windham, Connecticut for providing us with porcine ovarian tissue samples. Useful suggestions and technical support from engineers and personnel at Laser Components USA, Inc. and PicoLAS GmbH are also highly appreciated.

References

[1] L.V. Wang, S. Hu, Photoacoustic tomography: in vivo imaging from organelles to organs, Science (80-.) 335 (2012) 1458–1462. http://science.sciencemag.org/content/335/6075/1458.abstract.
[2] P. Beard, Biomedical photoacoustic imaging, Interface Focus 1 (2011) 602–631. http://rsfs.royalsocietypublishing.org/content/1/4/602.abstract.
[3] K. Maslov, L.V. Wang, Photoacoustic imaging of biological tissue with intensity-modulated continuous-wave laser, J. Biomed. Opt. 13 (2008) 24005–24006, doi:http://dx.doi.org/10.1117/1.2904965.
[4] G. Langer, B. Buchegger, J. Jacak, T.A. Klar, T. Berer, Frequency domain photoacoustic and fluorescence microscopy, Biomed. Opt. Express 7 (2016) 2692–2702, doi:http://dx.doi.org/10.1364/BOE.7.002692.
[5] C.L. Tsai, J.C. Chen, W.J. Wang, Near-infrared absorption property of biological soft tissue constituents, J. Med. Biol. Eng. 21 (2001) 7–14, doi:http://dx.doi.org/10.1016/j.jns.2015.02.025.
[6] J. Folkman, Role of angiogenesis in tumor growth and metastasis, Semin. Oncol. 29 (2002) 15–18, doi:http://dx.doi.org/10.1053/sonc.2002.37263.
[7] D.M. McDonald, P.L. Choyke, Imaging of angiogenesis: from microscope to clinic, Nat. Med. 9 (2003) 713–725.
[8] E.S. Bamberger, C.W. Perrett, Angiogenesis in epithelian ovarian cancer, Mol. Pathol. 55 (2002) 348.
[9] F. Hillen, A.W. Griffioen, Tumour vascularization: sprouting angiogenesis and beyond, Cancer Metastasis Rev. 26 (2007) 489–502.
[10] E. Lengyel, Ovarian cancer development and metastasis, Am. J. Pathol. 177 (2010) 1053–1064.
[11] K.S. Valluru, K.E. Wilson, J.K. Willmann, Photoacoustic Imaging in oncology: translational preclinical and early clinical experience, Radiology 280 (2016) 332–349.
[12] K.S. Valluru, J.K. Willmann, Clinical photoacoustic imaging of cancer, Ultrasonography 35 (2016) 267–280, doi:http://dx.doi.org/10.14366/usg.16035.
[13] M. Heijblom, D. Piras, W. Xia, J.C.G. van Hespen, J.M. Klaase, F.M. van den Engh, T.G. van Leeuwen, W. Steenbergen, S. Manohar, Visualizing breast cancer using the Twente photoacoustic mammoscope: what do we learn from twelve new patient measurements? Opt. Express 20 (2012) 11582, doi:http://dx.doi.org/10.1364/OE.20.011582.
[14] S.A. Ermilov, T. Khamapirad, A. Conjusteau, M.H. Leonard, R. Lacewell, K. Mehta, T. Miller, A.A. Oraevsky, Laser optoacoustic imaging system for detection of breast cancer, J. Biomed. Opt. 14 (2009) 24007.
[15] D.R. Bauer, R. Olafsson, L.G. Montilla, R.S. Witte, 3-D photoacoustic and pulse echo imaging of prostate tumor progression in the mouse window chamber, J. Biomed. Opt. 16 (2011) 26012.
[16] V.S. Dogra, B.K. Chinni, K.S. Valluru, J.V. Joseph, A. Ghazi, J.L. Yao, K. Evans, E.M. Messing, N.A. Rao, Multispectral photoacoustic imaging of prostate cancer: preliminary ex-vivo results, J. Clin. Imaging Sci. 3 (2013) 41, doi:http://dx.doi.org/10.4103/2156-7514.119139.
[17] M.A.L. Bell, N.P. Kuo, D.Y. Song, J. Kang, E.M. Boctor, In vivo photoacoustic imaging of prostate brachytherapy seeds, SPIE BiOS, International Society for Optics and Photonics (2014) 894348.
[18] Y. Zhou, W. Xing, K.I. Maslov, L.A. Cornelius, L.V. Wang, Handheld photoacoustic microscopy to detect melanoma depth in vivo, Opt. Lett. 39 (2014) 4731–4734.
[19] C.P. Favazza, O. Jassim, L.A. Cornelius, L.V. Wang, In vivo photoacoustic microscopy of human cutaneous microvasculature and a nevus, J. Biomed. Opt. 16 (2011) 16015–16016, doi:http://dx.doi.org/10.1117/1.3528661.
[20] C.P. Favazza, L.A. Cornelius, L.V. Wang, In vivo functional photoacoustic microscopy of cutaneous microvasculature in human skin, J. Biomed. Opt. 16 (2011) 26004–26005, doi:http://dx.doi.org/10.1117/1.3536522.
[21] J. Levi, S.-R. Kothapalli, S. Bohndiek, J.-K. Yoon, A. Dragulescu-Andrasi, C. Nielsen, A. Tisma, S. Bodapati, G. Gowrishankar, X. Yan, Molecular photoacoustic imaging of follicular thyroid carcinoma, Clin. Cancer Res. 19 (2013) 1494–1502.
[22] V.S. Dogra, B.K. Chinni, K.S. Valluru, J. Moalem, E.J. Giampoli, K. Evans, N.A. Rao, Preliminary results of ex vivo multispectral photoacoustic imaging in the management of thyroid cancer, Am. J. Roentgenol. 202 (2014) W552–W558.
[23] J.-M. Yang, C. Favazza, R. Chen, J. Yao, X. Cai, K. Maslov, Q. Zhou, K.K. Shung, L.V. Wang, Simultaneous functional photoacoustic and ultrasonic endoscopy of internal organs in vivo, Nat. Med. 18 (2012) 1297–1302, doi:http://dx.doi.org/10.1038/nm.2823.
[24] Y. Yuan, S. Yang, D. Xing, Preclinical photoacoustic imaging endoscope based on acousto-optic coaxial system using ring transducer array, Opt. Lett. 35 (2010) 2266–2268, doi:http://dx.doi.org/10.1364/OL.35.002266.
[25] M. Gerling, Y. Zhao, S. Nania, K.J. Norberg, C.S. Verbeke, B. Englert, R.V. Kuiper, Å. Bergström, M. Hassan, A. Neesse, J.M. Löhr, R.L. Heuchel, Real-time assessment of tissue hypoxia in vivo with combined photoacoustics and high-frequency ultrasound, Theranostics 4 (2014) 604–613, doi:http://dx.doi.org/10.7150/thno.7996.
[26] K. Peng, L. He, B. Wang, J. Xiao, Detection of cervical cancer based on photoacoustic imaging—the in-vitro results, Biomed. Opt. Express 6 (2015) 135–143, doi:http://dx.doi.org/10.1364/BOE.6.000135.
[27] T. Wang, Y. Yang, U. Alqasemi, P.D. Kumavor, X. Wang, M. Sanders, M. Brewer, Q. Zhu, Characterization of ovarian tissue based on quantitative analysis of photoacoustic microscopy images, Biomed. Opt. Express 4 (2013) 2763–2768, doi:http://dx.doi.org/10.1364/BOE.4.002763.
[28] H.S. Salehi, T. Wang, P.D. Kumavor, H. Li, Q. Zhu, Design of miniaturized illumination for transvaginal co-registered photoacoustic and ultrasound imaging, Biomed. Opt. Express 5 (2014) 3074–3079, doi:http://dx.doi.org/10.1364/BOE.5.003074.
[29] H.S. Salehi, P.D. Kumavor, H. Li, U. Alqasemi, T. Wang, C. Xu, Q. Zhu, Design of optimal light delivery system for co-registered transvaginal ultrasound and photoacoustic imaging of ovarian tissue, Photoacoustics 3 (2015) 114–122.
[30] H.S. Salehi, H. Li, A. Merkulov, P.D. Kumavor, H. Vavadi, M. Sanders, A. Kueck, M. A. Brewer, Q. Zhu, Coregistered photoacoustic and ultrasound imaging and classification of ovarian cancer: ex vivo and in vivo studies, J. Biomed. Opt. 21 (2016) 46006, doi:http://dx.doi.org/10.1117/1.JBO.21.4.046006.
[31] S.E. Bohndiek, L.S. Sasportas, S. Machtaler, J.V. Jokerst, S. Hori, S.S. Gambhir, Photoacoustic tomography detects early vessel regression and normalization during ovarian tumor response to the antiangiogenic therapy trebananib, J. Nucl. Med. 56 (2015) 1942–1947.
[32] P.D. Kumavor, U. Alqasemi, B. Tavakoli, H. Li, Y. Yang, X. Sun, E. Warych, Q. Zhu, Co-registered pulse-echo/photoacoustic transvaginal probe for real time imaging of ovarian tissue, J. Biophotonics. 6 (2013) 475–484.
[33] C.T.C. of America, Ovarian Cancer, (n.d.). www.cancercenter.com/ovarian (Accessed 16 May 2017).
[34] National ovarian cancer coalition, Types & Stages of Ovarian Cancer, (n.d.). http://www.ovarian.org/types_and_stages.php (Accessed 16 May 2017).
[35] W.A. Rocca, B.R. Grossardt, M. De Andrade, G.D. Malkasian, L.J. Melton, Survival patterns after oophorectomy in premenopausal women: a population-based cohort study, Lancet Oncol. 7 (2006) 821–828.
[36] C.T. Lam, M.S. Krieger, J.E. Gallagher, B. Asma, L.C. Muasher, J.W. Schmitt, N. Ramanujam, Design of a novel low cost point of care tampon (POCkeT) colposcope for use in resource limited settings, PLoS One 10 (2015) e0135869, doi:http://dx.doi.org/10.1371/journal.pone.0135869.
[37] M.N. Asiedu, J. Agudogo, M.S. Krieger, R. Miros, R.J. Proeschold-Bell, J.W. Schmitt, N. Ramanujam, Design and preliminary analysis of a vaginal inserter for speculum-free cervical cancer screening, PLoS One 12 (2017) e0177782, doi:http://dx.doi.org/10.1371/journal.pone.0177782.
[38] World Health Organisation, Compendium of Innovative Health Technologies for Low-resource Settings, World Health Organisation, Geneva, 2015. http://www.who.int/iris/handle/10665/202537.
[39] L. Zeng, G. Liu, D. Yang, X. Ji, 3D-visual laser-diode-based photoacoustic imaging, Opt. Express 20 (2012) 1237–1246.
[40] L. Zeng, G. Liu, D. Yang, X. Ji, Portable optical-resolution photoacoustic microscopy with a pulsed laser diode excitation, Appl. Phys. Lett. 102 (2013) 53704.
[41] T. Wang, S. Nandy, H.S. Salehi, P.D. Kumavor, Q. Zhu, A low-cost photoacoustic microscopy system with a laser diode excitation, Biomed. Opt. Express 5 (2014) 3053–3058.
[42] M. Erfanzadeh, H.S. Salehi, P. Kumavor, Q. Zhu, Improvement and evaluation of a low-cost laser diode photoacoustic microscopy system for ovarian tissue imaging, Proc. SPIE 9708, Photons Plus Ultrasound Imaging Sens. 2016 (2016), doi:http://dx.doi.org/10.1117/12.2208943 97083I–97083I–7.
[43] L. Zeng, Z. Piao, S. Huang, W. Jia, Z. Chen, Label-free optical-resolution photoacoustic microscopy of superficial microvasculature using a compact visible laser diode excitation, Opt. Express 23 (2015) 31026–31033.

[44] P.K. Upputuri, M. Pramanik, Performance characterization of low-cost, high-speed, portable pulsed laser diode photoacoustic tomography (PLD-PAT) system, Biomed, Opt. Express 6 (2015) 4118–4129.
[45] M.-L. Li, P.-H. Wang, Optical resolution photoacoustic microscopy using a Blu-ray DVD pickup head, SPIE BiOS, International Society for Optics and Photonics (2014) 894315.
[46] Q. Yao, Y. Ding, G. Liu, L. Zeng, Low-cost photoacoustic imaging systems based on laser diode and light-emitting diode excitation, J. Innov. Opt. Health Sci. 10 (2017) 1730003, doi:http://dx.doi.org/10.1142/S1793545817300038.
[47] Julie Randolph-Habecker, Tips about Fixation and Formalin, (n.d.). https://sharedresources.fredhutch.org/training/tips-about-fixation-and-formalin (Accessed 20 May 2017).
[48] K.B. Roth, K.B. Neeves, J. Squier, D.W.M. Marr, Imaging of a linear diode bar for an optical cell stretcher, Biomed. Opt. Express 6 (2015) 807–814.
[49] B.H. Hasegawa, The Physics of Medical X-ray Imaging, Medical Physics Publishing Corporation, Madison, 1990.
[50] S.W. Smith, The Scientist and Engineer's Guide to Digital Signal Processing, California Technical Pub, San Diego, 1997.
[51] C. Zhang, K. Maslov, J. Yao, L.V. Wang, In vivo photoacoustic microscopy with 7.6-(m axial resolution using a commercial 125-MHz ultrasonic transducer, J. Biomed. Opt. 17 (2012) 116016.
[52] A.J. LeBlanc, L. Krishnan, C.J. Sullivan, S.K. Williams, J.B. Hoying, Microvascular repair post-angiogenesis vascular dynamics, Microcirculation 19 (2012) 676–695.
[53] P.J. Van Diest, J.P. Zevering, L.C. Zevering, J.P.A. Baak, Prognostic value of microvessel quantitation in cisplatin treated FIGO 3 and 4 ovarian cancer patients, Pathol. Pract. 191 (1995) 25–30.
[54] V.G. Djonov, H. Kurz, P.H. Burri, Optimality in the developing vascular system: branching remodeling by means of intussusception as an efficient adaptation mechanism, Dev. Dyn. 224 (2002) 391–402, doi:http://dx.doi.org/10.1002/dvdy.10119.
[55] L.A. Martinez-Lemus, The dynamic structure of arterioles, Basic Clin. Pharmacol. Toxicol. 110 (2012) 5–11, doi:http://dx.doi.org/10.1111/j.1742-7843.2011.00813.x.
[56] P.K. Yu, D. Yu, V.A. Alder, U. Seydel, E. Su, S.J. Cringle, Heterogeneous endothelial cell structure along the porcine retinal microvasculature, Exp. Eye Res. 65 (1997) 379–389, doi:http://dx.doi.org/10.1006/exer.1997.0340.
[57] J. Yao, L. Wang, J.-M. Yang, K.I. Maslov, T.T.W. Wong, L. Li, C.-H. Huang, J. Zou, L. V. Wang, High-speed label-free functional photoacoustic microscopy of mouse brain in action, Nat. Methods 12 (2015) 407–410.
[58] Z. Xie, S. Jiao, H.F. Zhang, C.A. Puliafito, Laser-scanning optical-resolution photoacoustic microscopy, Opt. Lett. 34 (2009) 1771–1773, doi:http://dx.doi.org/10.1364/OL.34.001771.
[59] E.W. Stein, K. Maslov, L.V. Wang, Noninvasive, in vivo imaging of the mouse brain using photoacoustic microscopy, J. Appl. Phys. 105 (2009) 102027.
[60] H.F. Zhang, K. Maslov, G. Stoica, L.V. Wang, Functional photoacoustic microscopy for high-resolution and noninvasive in vivo imaging, Nat. Biotechnol. 24 (2006) 848–851, doi:http://dx.doi.org/10.1038/nbt1220.
[61] H.F. Zhang, K. Maslov, M.-L. Li, G. Stoica, L.V. Wang, In vivo volumetric imaging of subcutaneous microvasculature by photoacoustic microscopy, Opt. Express 14 (2006) 9317–9323, doi:http://dx.doi.org/10.1364/OE.14.009317.
[62] M. Sánchez, S. Rodríguez, L. Leggio, S. Gawali, D. Gallego, H. Lamela, Beam profile improvement of a high-power diode laser stack for optoacoustic applications, Int. J. Thermophys. 38 (2017) 48, doi:http://dx.doi.org/10.1007/s10765-017-2182-1.
[63] P. Hai, J. Yao, K.I. Maslov, Y. Zhou, L.V. Wang, Near-infrared optical-resolution photoacoustic microscopy, Opt. Lett. 39 (2014) 5192–5195, doi:http://dx.doi.org/10.1364/OL.39.005192.
[64] T.J. Allen, P.C. Beard, High power visible light emitting diodes as pulsed excitation sources for biomedical photoacoustics, Biomed. Opt. Express 7 (2016) 1260–1270.
[65] X. Dai, H. Yang, H. Jiang, In vivo photoacoustic imaging of vasculature with a low-cost miniature light emitting diode excitation, Opt. Lett. 42 (2017) 1456–1459, doi:http://dx.doi.org/10.1364/OL.42.001456.
[66] L.E. Horvath, T. Werner, K. Boucher, K. Jones, The relationship between tumor size and stage in early versus advanced ovarian cancer, Med. Hypotheses 80 (2013) 684–687, doi:http://dx.doi.org/10.1016/j.mehy.2013.01.027.
[67] S. Hu, K. Maslov, L.V. Wang, Second-generation optical-resolution photoacoustic microscopy with improved sensitivity and speed, Opt. Lett. 36 (2011) 1134, doi:http://dx.doi.org/10.1364/OL.36.001134.
[68] NDT resource center, signal-to-noise ratio, (n.d.). https://www.nde-ed.org/EducationResources/CommunityCollege/Ultrasonics/Physics/signaltonoise.htm (Accessed 5 September 2017).
[69] A.N.S. Institute, American National Standard for Safe Use of Lasers, Laser Institute of America, 2007.
[70] M. Luciano, M. Erfanzadeh, F. Zhou, H. Zhu, T. Bornhutter, B. Roder, Q. Zhu, C. Bruckner, In vivo photoacoustic tumor tomography using a quinoline-annulated porphyrin as NIR molecular contrast agent, Org. Biomol. Chem. 15 (2017) 972–983, doi:http://dx.doi.org/10.1039/C6OB02640K.
[71] L. Leggio, S. Gawali, D. Gallego, S. Rodríguez, M. Sánchez, G. Carpintero, H. Lamela, Optoacoustic response of gold nanorods in soft phantoms using high-power diode laser assemblies at 870 and 905 nm, Biomed. Opt. Express 8 (2017) 1430–1440.
[72] R.J. Paproski, A. Forbrich, E. Huynh, J. Chen, J.D. Lewis, G. Zheng, R.J. Zemp, Porphyrin nanodroplets: sub-micrometer ultrasound and photoacoustic contrast imaging agents, Small 12 (2016) 371–380, doi:http://dx.doi.org/10.1002/smll.201502450.
[73] J. Weber, P.C. Beard, S.E. Bohndiek, Contrast agents for molecular photoacoustic imaging, Nat. Methods 13 (2016) 639–650, doi:http://dx.doi.org/10.1038/nmeth.3929.
[74] D. Wu, L. Huang, M.S. Jiang, H. Jiang, Contrast agents for photoacoustic and thermoacoustic imaging: a review, Int. J. Mol. Sci. 15 (2014) 23616–23639.
[75] Y. Jin, X. Ma, S. Zhang, H. Meng, M. Xu, X. Yang, W. Xu, J. Tian, A tantalum oxide-based core/shell nanoparticle for triple-modality image-guided chemo-thermal synergetic therapy of esophageal carcinoma, Cancer Lett. 397 (2017) 61–71, doi:http://dx.doi.org/10.1016/j.canlet.2017.03.030.

Mohsen Erfanzadeh received his B.S in Physics from University of Tehran, Iran and M.S in Photonics from Shahid Beheshti University, Iran. He is currently pursuing his PhD in Biomedical Engineering at University of Connecticut, USA. His research interest includes design and development of novel optical imaging systems for clinical and pre-clinical applications.

Patrick D. Kumavor holds a Ph.D. in Electrical Engineering from the University of Connecticut. In addition, he also has a B.S. in Physics and M.S. in Biomedical Engineering. Patrick has worked on a diverse array of research topics ranging from all-optical signal processing, through quantum cryptography, to biomedical imaging. His most recent research work is the development of novel photoacoustic imaging systems using fiber-optic technologies for early-stage cancer detection.

Quing Zhu Joined Washington University in St.Louis as a professor of the Department of Biomedical Engineering and Radiology in July 2016. Previously, she was a professor of Electrical and Computer Engineering at the University of Connecticut. She has been named fellow of Optical Society of America, and fellow of SPIE. Her research is focused on ultrasound and optical techniques for breast and ovarian cancer diagnosis and treatment monitoring. Recently, she has started collaborations with the excellent physicians at Washington University in St. Louis on colorectal and cervical cancer treatment prediction and monitoring.